

# Supporting Information for

## Effects of aqueous buffers on electrocatalytic water oxidation with an iridium oxide material electrodeposited in thin layers from an organometallic precursor

*Maxwell N. Kushner-Lenhoff,<sup>†</sup> James D. Blakemore,<sup>‡</sup> Nathan D. Schley, Robert H. Crabtree,\* and Gary W. Brudvig\**

Department of Chemistry, Yale University, P.O. Box 208107,  
New Haven, Connecticut 06520-8107

E-mail: gary.brudvig@yale.edu (G.W.B.); robert.crabtree@yale.edu (R.H.C.)

<sup>†</sup> Current address: Dow Chemical Company, 450 Park Avenue Suite 2200, New York, New York 10022

<sup>‡</sup> Current address: Beckman Institute, and Division of Chemistry and Chemical Engineering, California Institute of Technology, MC 139-74, Pasadena, California 91125

| <b><u>Index</u></b>             | <b><u>Page</u></b> |
|---------------------------------|--------------------|
| Experimental Methods            | S2-S3              |
| Additional electrochemical data | S4-S8              |
| Oxygen evolution data           | S9                 |
| References                      | S10                |

## Experimental Methods

All reagents were purchased from major commercial suppliers and used as received. MilliQ water was used to prepare all aqueous solutions.

## Sample Preparation

Compound **1** was synthesized according to literature procedures.<sup>1</sup> For catalyst electrodeposition, 1.72 mM solutions of **1** were prepared in 0.1 M KNO<sub>3</sub> electrolyte. To ensure maximum reproducibility, depositions were each conducted with a fresh portion of catalyst precursor solution in all experiments where a quantitative effect on overpotential was measured, and also for all experiments with Na<sub>2</sub>SiF<sub>6</sub>.

Unless noted otherwise, the buffering solutions contained both the buffer and 0.1 M KNO<sub>3</sub> electrolyte. (In some preliminary studies, the working solution did not contain KNO<sub>3</sub>.) Additional electrolyte does not have an observable effect on the results in the cases where the buffer concentration or salt concentration is near or above 0.1 M.

The pH of the buffered solutions was monitored with a Corning PerpHect pH electrode. In some cases, the pH of the solutions was adjusted by addition of dilute HNO<sub>3</sub> or KOH, as needed.

## Electrochemistry

Electrochemical measurements were made on a Princeton Applied Research Versastat 4-400 potentiostat/galvanostat using a standard single-chamber three-electrode configuration. A Ag/AgCl reference electrode (Ag/AgCl vs. NHE = +197 mV) and platinum counter electrode were used in all experiments unless noted otherwise. The electrochemical cell was a small three-neck flask with two of the three necks threaded to hold the counter and working electrodes in place. The working electrode was a platinum rotating-disk electrode (RDE) (Pine E3; Pt disk in teflon casing) (surface area: 0.196 cm<sup>2</sup>).

All experiments characterizing electrocatalyst activity were performed using thin preparations of **BL** deposited by ten cycles of voltammetry from 0.2 to 1.5 V vs. NHE at a scan rate of 50 mV/s. **BL** was electrodeposited onto the stationary platinum rotating-disk electrode, which served as the working electrode.

To avoid mass transport limitations, Tafel plots were generated with electrode rotation using a Princeton Applied Research Model 616 variable-speed rotator. Although the RDE was stationary during deposition, it was rotated at 1500 rpm during the collection of Tafel data. This rate was found to allow water oxidation to occur without significant mass transport limitations. However, it was not sufficient to overcome all mass transport limitations, as faster rotation speeds gave higher sustained currents at the highest overpotentials.

Preliminary Tafel plots were collected from low-to-high applied potential in 50 mV steps with a dwell time of 300 sec. Some more detailed studies (the phosphate concentration dependence and trifluoromethanesulfonamide work) were done with potentials increasing in 25 mV steps and with 150 sec dwell time. Current densities reported in the paper are calculated based on observed current at the end of each potential step.

Overpotential data (e.g., Figure 1) were calculated using the difference between the pH-adjusted thermodynamic potential for water oxidation ( $E^{\circ'}$ ) and the applied potential required to achieve a steady-state current of 0.5 mA cm<sup>-2</sup>.

Error bars reflect the error of replicate electrochemical measurements for the thin layers of catalyst being used and likely represent an overestimate. No correction has been made here for uncompensated cell resistance (i.e., iR drop).

### **Oxygen Evolution**

A YSI Clark-type oxygen electrode was used to detect oxygen evolved during electrochemically-driven water oxidation as described previously.<sup>2</sup> The Clark electrode was placed in a custom water-jacketed glass vessel that allows for working, reference, and counter electrodes to be fitted with an O-ring and inserted using screw-in plastic caps. The working electrode was a stationary platinum disk electrode (surface area: 0.017 cm<sup>2</sup>). Magnetic stirring was used to ensure that the solution was mixed. Electrochemical data collected during oxygen detection were, however, limited by mass transport and are, therefore, not strictly comparable to buffering results using the RDE.

## Additional Tafel Plots

**Figure S1.** Tafel plot data for preparation of Figure 1.

With phosphate as buffer (upper panel; solid points), the expected pH dependence was observed (i.e., the overpotential is essentially invariant with pH, shifting by approximately 59 mV per pH unit). In the absence of phosphate (lower panel; unfilled squares), the overpotential is pH dependent and increases as the solution pH is increased.

We also note the increased overpotential at pH 4 in the presence of dilute phosphate. It seems that, under these conditions, phosphate is inactive as a buffer but may still coordinate to catalytic sites, resulting in a net deleterious effect.

Phosphate buffer concentration was 5 mM.

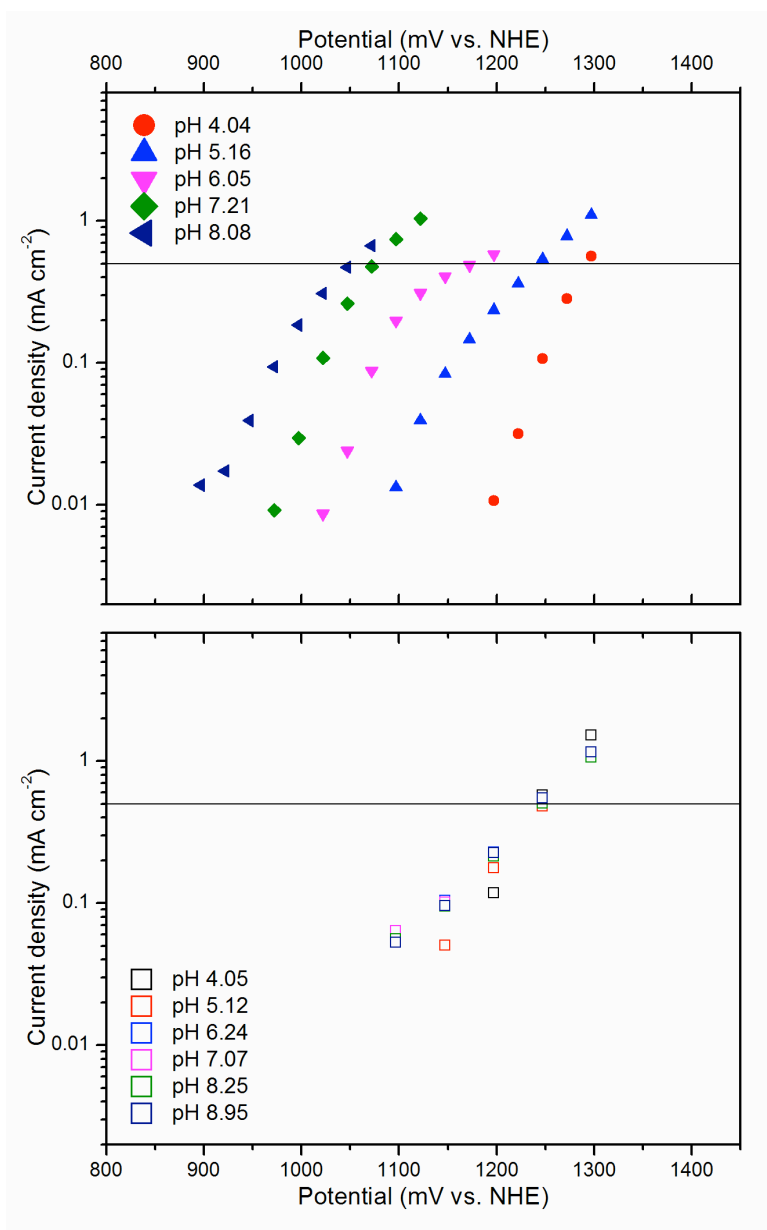


**Figure S2.** Tafel plot for  $\text{Na}_2\text{SiF}_6$  as buffer.

Buffer studies were performed using  $\text{Na}_2\text{SiF}_6$ , previously found by Mallouk *et al.* to be effective in the case of iridium oxide nanoparticles.<sup>3</sup> In this system,  $\text{HF}/\text{F}^-$  (formed *in situ*) acts as the buffering agent and has a  $\text{pK}_a$  of 3.5.<sup>4</sup> Due to complications from the HF, a platinum wire previously referenced versus  $\text{Ag}/\text{AgCl}$  was used as the reference electrode for these experiments. Unlike in the case of the iridium oxide nanoparticles,  $\text{Na}_2\text{SiF}_6$  was found to be ineffective for the **BL** system.

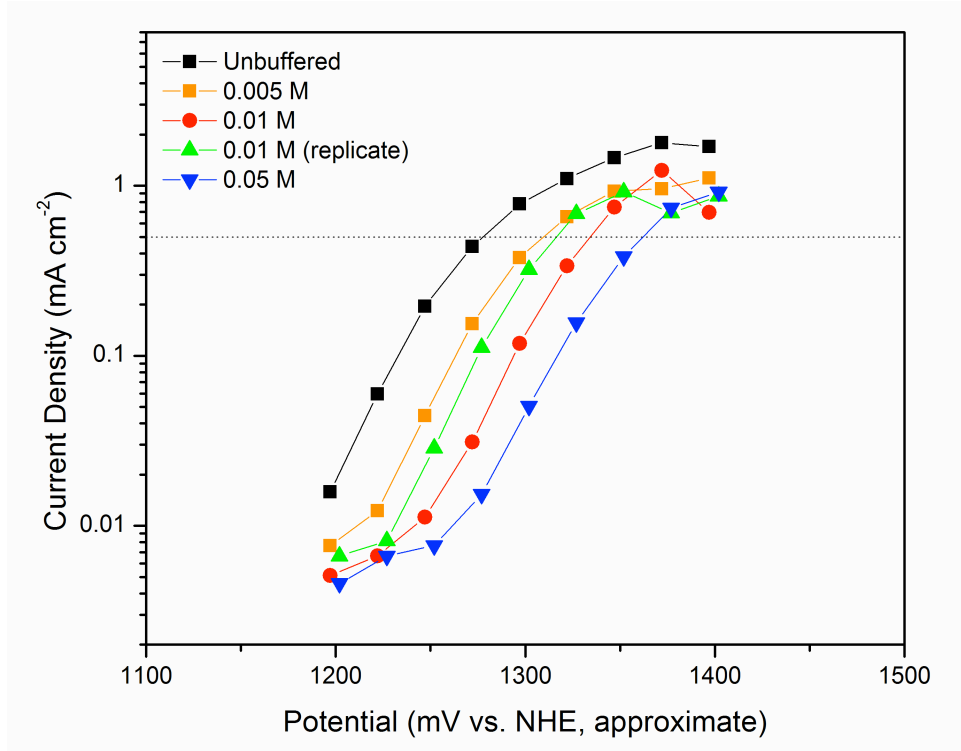


**Figure S3.** Tafel plot for acetate buffer

Within the buffering range of acetate ( $\text{pH} = 4.75 \pm 0.5$ ), the current density was pH-dependent but was not improved markedly versus the unbuffered case. Acetate buffer also causes corrosion at current densities of as low as  $0.5 \text{ mA cm}^{-2}$ , resulting in loss of activity as shown below.

Red vertical line indicates  $E^{0'}$  of 950 mV vs. NHE at pH 4.75.

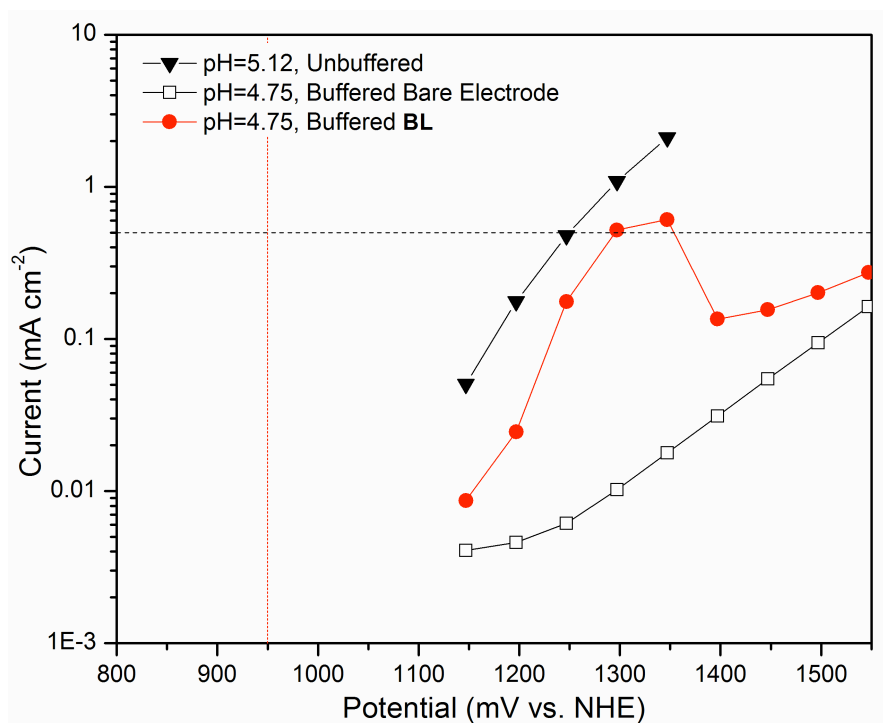


**Figure S4.** Tafel plot for dilute bicarbonate

Dilute bicarbonate buffer was shown to decrease observed overpotential by 60 mV, but the Tafel plot has the same slope as unbuffered electrolyte, suggesting that there is no change in mechanism. Thus, the observed effect is attributed to bicarbonate's role in countering local pH effects.

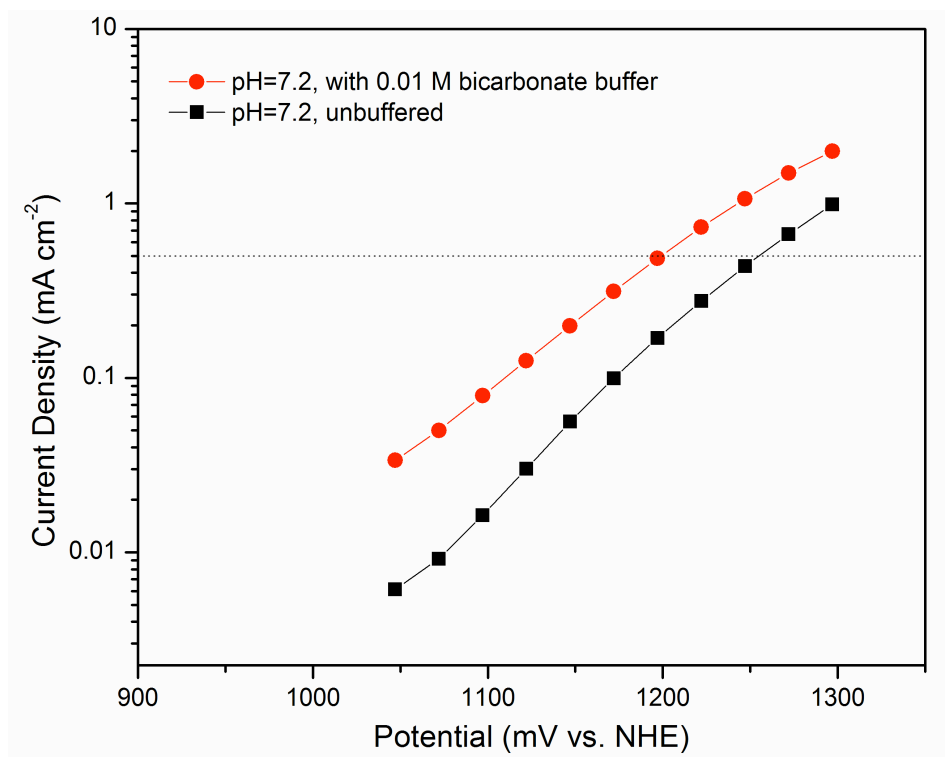


**Figure S5.** Tafel plot for trifluoromethanesulfonamide (TFMS) as buffer.

At a pH of 6.33 (the lower  $pK_a$  of TFMS) in 0.1 M  $KNO_3$  solution and 10 mM TFMS, the current response shows an apparent buffered overpotential of 139 mV less than the unbuffered case (255 mV vs. 394). However, as is evident from the oxygen evolution data (see below), some of this increased current flow is attributed to oxidative degradation of the buffer.

Also of note is the observation that TFMS causes corrosion at current densities above  $0.5 \text{ mA cm}^{-1}$ , which could be due to catalyst fouling.

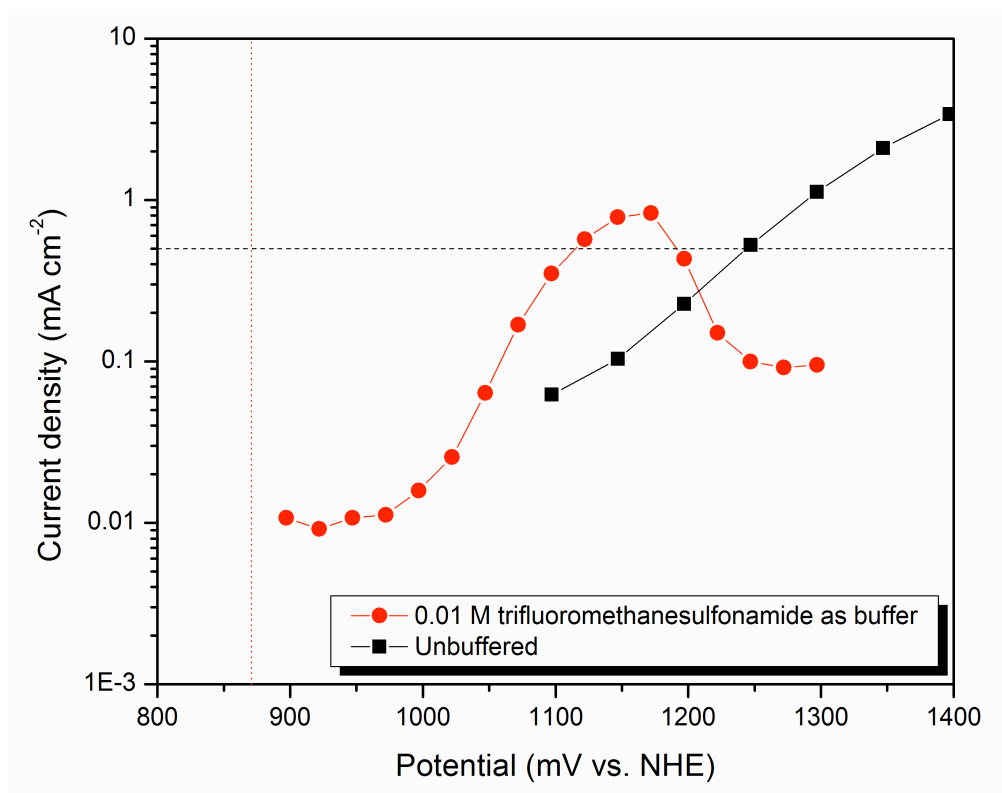
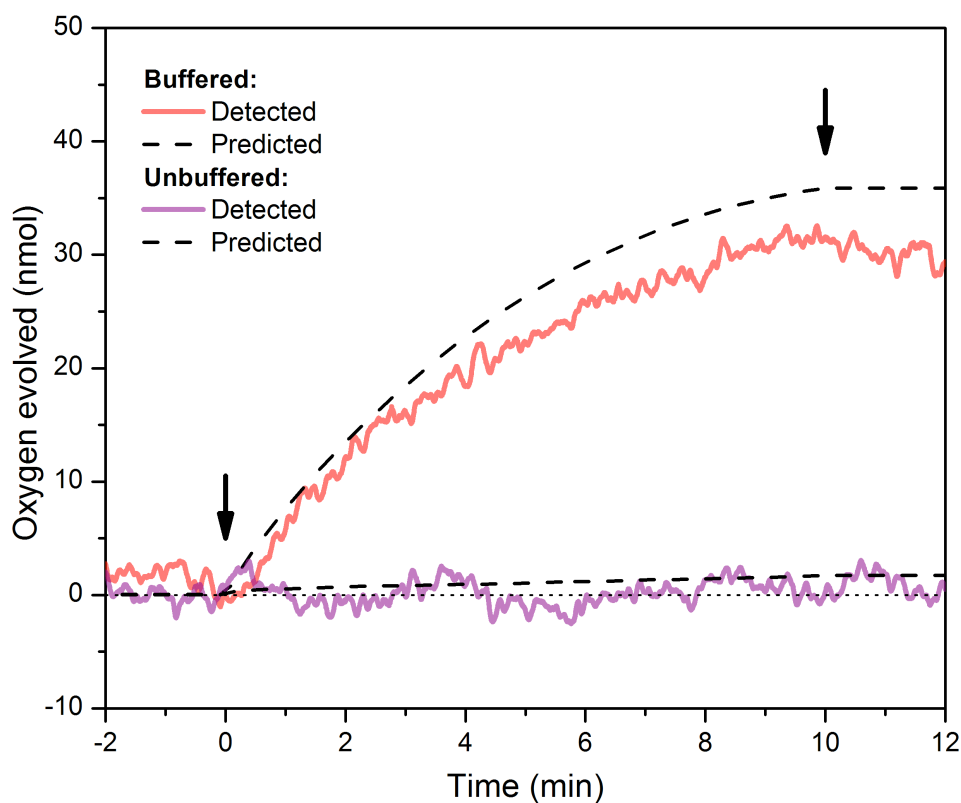


**Figure S6.** Comparison of oxygen evolution in unbuffered electrolyte electrolyte buffered with trifluoromethanesulfonamide (TFMS)

Oxygen evolution data with 50 mM TFMS at 1.12 V vs. NHE show decreasing oxygen-evolution activity over the course of the 10-minute experiment. This decrease in catalytic activity can be attributed to deactivation of the catalyst under the experimental conditions. In addition, the O<sub>2</sub> yield of this experiment was only 88% of that predicted based on current flow, showing that some current was consumed in an unproductive pathway, most likely oxidative degradation of the TFMS buffer.

Black arrows show start and stop of the electrode polarization at time zero and after 10 minutes.

As in the case of phosphate (Figure 4), essentially no oxygen is evolved in the absence of the buffer.



## References

- <sup>1</sup> Ogo, S.; Makihara, N.; Watanabe, Y. *Organometallics* **1999**, *18*, 5470-5474.
- <sup>2</sup> (a) Schley, N. D.; Blakemore, J. D.; Subbaiyan, N. K.; Incarvito, C. D.; D'Souza, F.; Crabtree, R. H.; Brudvig, G. W. *J. Am. Chem. Soc.* **2011**, *133*, 10473–10481. (b) Blakemore, J. D.; Schley, N. D.; Kushner-Lenhoff, M. N.; Winter, A. M.; D'Souza, F.; Crabtree, R. H.; Brudvig, G. W. *Inorg. Chem.* **2012**, *51*, 7749. (c) Blakemore, J. D.; Smith, D. M. *Fusion: J. Am. Scientific Glassblowers Soc.* **2012**, *51* (2), 21-27.
- <sup>3</sup> (a) Hara, M.; Waraksa, C. C.; Lean, J. T.; Lewis, B. A.; Mallouk, T. E. *Journal of Physical Chemistry A* **2000**, *104*, 5275. (b) Hoertz, P. G.; Kim, Y.-I.; Youngblood, W. J.; Mallouk, T. E. *J. Phys. Chem. B* **2007**, *111*, 6845–6856.
- <sup>4</sup> Mellor, J. W. *A Comprehensive Treatise on Inorganic and Theoretical Chemistry*; Longmans, Green & Co.: New York, 1925; vol. 6, page 943.